NASA TECHNICAL MEMORANDUM

NASA TM X-73627

NASA TM X-73627

TECHNIQUES FOR INCREASING BORON FIBER FRACTURE STRAIN

by J. A. DiCarlo
Lewis Research Center
Cleveland, Ohio 44135

TECHNICAL PAPER to be presented at the
One hundred sixth Annual Meeting of the
American Institute of Mining, Metallurgical, and Petroleum Engineers
Atlanta, Georgia, March 6-10, 1977

TECHNIQUES FOR INCREASING BORON FIBER FRACTURE STRAIN

by J. A. DiCarlo

Lewis Research Center
Cleveland, Ohio 44135

ABSTRACT

Improvement in the strain-to-failure of CVD boron fibers is shown possible by contracting the tungsten boride core region and its inherent flaws. The results of three methods are presented in which etching and thermal processing techniques were employed to achieve core flaw contraction by internal stresses available in the boron sheath. After commercially and treatment-induced surface flaws were removed from 203 μm (8 mil) fibers, the core flaw was observed to be essentially the only source of fiber fracture. Thus, fiber strain-to-failure was found to improve by an amount equal to the treatment-induced contraction on the core flaw. To date, average fracture strains and stresses greater than 1.4 percent and 5.5 GN/m^2 (800 ksi), respectively, have been achieved. Commercial feasibility considerations suggest as the most cost-effective technique that method in which as-produced fibers are given a rapid heat treatment above 700° C. Preliminary results concerning the contraction kinetics and fracture behavior observed with this technique are presented and discussed both for high vacuum and argon gas heat treatment environments.

E-9119

STAR Category 24

INTRODUCTION

Boron fibers employed as composite reinforcement offer the significant advantages of high modulus, high strength, and low density. Although these properties may be more than sufficient in many design situations, the present day strength of commercial boron fibers (3.5 GN/m^2) is much less than optimum due to flaws introduced in the fiber manufacturing process. This reduced strength becomes especially critical in those composite areas where high strain-to-failure and high impact resistance are required. Thus, if the full capabilities of boron fibers are to be achieved, attempts must be made to optimize fiber strength and fracture strain by either eliminating flaws or minimizing their effects.

The process of flaw elimination is complicated by the many variables existing in the formation of boron fibers by chemical vapor deposition (CVD) on a tungsten wire substrate. Over the last decade or so, gradual improvements have been made to the point that the major flaws are now located only at the fiber surface and at the borided tungsten core (1, 2). Smith (2) has shown that the surface flaws can be eliminated by a simple chemical etch, increasing average strength to over 4.4 GN/m^2 and decreasing strength coefficient-of-variability from 20 percent to less than 5 percent. Although this improvement is significant by design standards, Wawner and Satterfield (1) have demonstrated that if the core flaw could be eliminated, average strengths over 7 GN/m^2 should be obtainable.

Because the core and probably its inherent flaws are such an integral part of current fiber manufacturing techniques, it is desirable at the present time to develop alternate methods in which the core is retained but its effects on fiber strength are minimized. In this report the results of three such minimization techniques will be presented and discussed. One technique (etch) was employed by Smith (2) in which he observed a gradual increase in fiber strength upon etching toward the core. Behrendt (3) has shown that this increase can be explained entirely by a residual stress pattern which contracts the fiber and elastically compresses the core flaw as outer boron surface layers are removed. The fiber fracture strain is thus increased by

the corresponding increment of contraction exerted on the core flaw. Recently, DiCarlo (4) has suggested thermal techniques to take advantage of the deformation character of the boron sheath to achieve core flaw contraction and fiber strain-to-failure improvement. The results of one of these techniques (etch-heat) will be presented here, along with preliminary findings on a newly developed high temperature contraction technique (heat-etch) which may yield fiber strengths above 7 GN/m^2 without core flaw elimination.

PROCEDURE AND RESULTS

The principal specimens of this study were 203 μm (8 mil) diameter fibers commercially supplied by Avco Systems Division. These fibers were produced in a single stage reactor by the hydrogen reduction of boron trichloride on a 13 μm (0.5 mil) tungsten wire substrate held near 1300° C. Fibers from the same commercial run were also employed by Smith for his study of the effects of etching on fracture strength (2), by Behrendt for his measurements of residual stress patterns (3), and by DiCarlo for his determination of the time, temperature, and stress dependence of boron fiber deformation (4, 5). From these studies emerges a low temperature deformation model of the fiber consisting of a 17 μm elastic tungsten-boride core surrounded by a 203 μm anelastic boron sheath. Smith found that after etching a few μm off the surface of the as-received fibers, essentially all cases of fracture could be explained by crack initiation near the region of the core. Apparently after surface removal, those flaws that remained in the boron sheath could not initiate fracture at the level of the core flaw.

Regarding fracture parameters, DiCarlo (4) has shown that due to the anelastic nature of the boron sheath, the fiber fracture strength σ_F is a function of test conditions. That is, σ_F depends on time t, temperature T, and fiber fracture strain ϵ_F according to the relation:

$$\sigma_F(t,T) = \frac{\epsilon_F E(T)}{A_H(q)} \tag{1}$$

Here $E(T)$ is the temperature-dependent elastic modulus of the boron sheath and $A_H(q)$ is the high stress anelastic strain function of the sheath as shown Fig. 1. The parameter q contains both the temperature (^{O}K) and the length of time (sec) of the stress application; i.e.,

$$q = (\ln t + 33.7)T(10^{-3}) \tag{2}$$

It is clear from Eq. (1) and Fig. 1 that for constant fracture strain, σ_F may vary by over a factor of two depending on test conditions. For this reason, in the discussions that follow, the parameter fracture strain rather than fracture stress will be emphasized whenever improvements in fiber fracture conditions are considered.

Etch Technique

This technique employed by Smith (2) consists simply of removing outer sheath layers from commercial 203 μm (8 mil) boron fibers. In his work Smith measured fracture strength as a function of fiber diameter after chemically etching in a solution of one part fuming nitric acid and one part water. Near 100^{O} C the surface removal rate was about 25 μm (1 mil) off the diameter in 5 min. In order to convert Smith's σ_F data to ϵ_F data using Eq. (1), optical elongation measurements were made as a function of high stress for approximately the same fracture time (~400 sec) and temperature (295^{O} K) conditions ($q_0 = 12$) employed by Smith. For several specimens ~80 mm in length, the average of the quantity $E/A_H(q_0)$ was 392 GN/m^2 (56.8 Msi). This value inserted in Eq. (1) yields the band of fracture strain data shown in Fig. 2 as a function of etched diameter down to 100 μm.

Clearly the etch technique had two important effects on fiber fracture strain. First, there was the sharp rise in ϵ_F achieved simply by the

removal of only a few μm off the original diameter. Obviously surface flaws are an on-going problem with present-day commercial fibers and necessarily must be eliminated before any significant improvements in fiber fracture conditions are to be achieved. Once surface flaws were removed, optical examination of fracture surfaces clearly indicated the core region as the source of fracture in the etched fiber. This observation was supported by the independence on diameter of the fracture strain band width shown in Fig. 2. Thus the fracture strain of a slightly etched fiber can be attributed directly to the fracture strain of its core flaw. That is, after surface flaw elimination the fiber fractures whenever its deformation strain reaches the core flaw fracture strain ϵ_F^c.

The second effect of the etch technique was to gradually increase ϵ_F^c as diameters were reduced well below the original diameter. Near 203 μm, for example, average ϵ_F^c was determined to be 1.11 %; whereas near 100 μm this parameter had increased to 1.3 %. This improvement has been explained by Behrendt (3) in terms of an interaction between the core flaw and the residual stress pattern inherent to CVD boron fibers. This pattern as determined by Behrendt (6) for a typical Avco 203 μm fiber is shown in Fig. 3, curve A. As indicated, the surface layers of the as-produced fiber are under compression, the center layers under tension, and the layers near and at the core under compression. This pattern was obtained by electropolishing the fibers at room temperature and simultaneously observing the axial strain as a function of surface removal. The strain data corresponding to curve A of Fig. 3 are shown in curve A of Fig. 4. Thus, down to 100 μm the axial strain is contractive (negative sign), so that additional compression is exerted on the core flaw by the surface removal process. If the core flaw is assumed to deform elastically this contractive strain can be added to the initial ϵ_F^c to yield the dashed line of Fig. 2. The agreement between this line and Smith's average fracture data confirms the model in which the fiber fracture strain is determined by the core flaw fracture strain as modified by sheath stresses. The validity of this model is also indicated in Table I where the results of etch technique for both 198 and 102 μm etched diameters are compared

in terms of the change in the average core fracture strain $\overline{\Delta\epsilon_F^c}$ and the average measured fiber axial contraction $\bar{\epsilon}_z$.

It should be mentioned at this point that whenever techniques discussed in this paper required surface removal to improve fracture strain, a practical lower limit of 100 μm was set on the final fiber diameter. This limit was based on three observations. First, the as-produced 102 μm (4 mil) fiber is the smallest diameter fiber currently receiving considerable commercial application. Second, as evident in curve A of Fig. 4, surface removal below the 100 μm level will tend to elongate the fiber, thereby diminishing the core flaw contraction effects already gained. Third, as fiber surfaces are removed, the axial stress state on the newly exposed surface diminishes in compression. Behrendt's (6) determination of the surface stress state with continuous electropolishing is shown by curve B of Fig. 3. Due to fiber contraction this surface stress is more compressive than curve A and therefore does not go into tension until near 100 μm. Thus, on the premise that a tensile surface state contributes more to notch sensitivity, final diameters below 100 μm should be more prone to surface flaws introduced by handling. Indeed, Smith suggested this effect as a possible source for the random appearance of low strength fibers at etched diameters below 80 μm.

Etch-Heat Technique

The residual stress pattern in CVD boron fibers is the result of conditions existing during high temperature deposition plus possible effects of quenching down to low temperature after deposition. Without attempting to derive an exact deformation theory to explain the details of Fig. 3, one can envision a phenomenological model in which during fiber production each boron layer is somehow deposited in a compressive state. The added layer tends to force inside layers into tension in order to achieve force equilibrium. Thus as deposition proceeds layers within the surface experience increasing tensile force. The magnitude of this tensile component depends on the layer location at final quench and the time, temperature, and stress-dependent

creep characteristics of the CVD boron. Indeed, both Behrendt (3) and Witucki (7) have argued that creep must occur; otherwise significantly greater tensile stresses would be observed for the inner regions.

Regarding CVD boron creep behavior, DiCarlo (4) has demonstrated that at any temperature the initial deformation is characteristically anelastic. That is, a boron layer subjected to a tensile stress will exhibit in the first instants of time a deformation strain consisting of an elastic component and an anelastic component ϵ_a. This latter component is initially zero but grows with time, temperature, and stress according to the relation

$$\epsilon_a(t, T, \sigma) = \sigma \left[A(q) - 1\right]/E(T) \tag{3}$$

Another significant property of anelastic behavior is the property of creep recovery or elastic aftereffect. That is, upon stress removal the developed anelastic strain component disappears at a rate dependent on time and temperature.

The etch-heat technique is therefore based on the model that layers within the surface of the as-received fibers must have undergone axial anelastic tensile creep during the CVD process. When any outer boron layers providing some part of this tensile deformation are removed, e.g., by etching, both the elastic and anelastic axial strain components will be permitted to disappear. This in turn allows the fiber to contract, thereby increasing the core flaw fracture strain. Near room temperature, DiCarlo has shown that anelastic creep and thus anelastic recovery is imperceptibly slow. Therefore Behrendt's axial contraction results of curve A Fig. 4 can be considered to be caused by the disappearance of only elastic strain. However, if the residual stress experiment were performed at higher temperature where anelastic strain recovery can measurably occur within the time framework of the experiment, axial contraction should then be higher than that indicated in Fig. 4. This higher contraction should increase core fracture strain provided that at the high temperature (a) the core flaw behaves elastically, (b) the final ϵ_F^c does not exceed ϵ_F of flaws already existing

in the boron sheath, and (c) no new low strain surface or bulk flaws are introduced by the heat treatment method.

Requirements of the etch-heat technique are therefore either to etch at high temperature or to etch at low temperature and then heat to high temperature. The latter approach was employed here in which a batch of ~80 mm long as-received fibers were chemically etched in the manner employed by Smith and then given a high temperature heat treatment in a high vacuum environment. A schematic of the apparatus employed for heating a batch of some 40 fibers in a vacuum less than 10^{-7} mm Hg is shown in Fig. 5. Before and after heating, the length of some of the etched fibers was measured to ±0.003 mm with a traveling microscope in order to verify the anelastic contraction effect. The average axial contraction strain for 203 μm fibers etched to 104 μm is shown by curve A in Fig. 6 for 60 min thermal treatments above 500° C. It should be pointed out that in effect these fibers were already heat treated near 100° C by the chemical etch process so that no heat-induced strain should have been observed until treatment temperatures above 100° C were employed.

After the etch-heat treatment, fiber fracture stresses were measured under the same test conditions employed by Smith ($q_0 = 12$). The average fracture stress and strain results after various heat treatments are given in Table I under the Etch-Heat heading. In this table, D_1 is the etched fiber diameter before heat treatment. Because of the low variation in core flaw fracture strain, only 10 etched specimens were employed for each heat treatment run. However, the number of specimens available for fracture measurements sometimes diminished to 4 due to surface problems encountered at high temperature. For example, above 700° C it was observed that both for the as-received and etched fibers boron crystals would grow on the fiber surface. A scanning electron microscope photograph of these crystals is shown in Fig. 7. Since these crystals had a significantly lower ϵ_F than the core flaw, it was necessary to subject the fibers to a second etch down to the final diameter D_2 given in Table I. The depth of surface removal required to eliminate the crystals and assure core-initiated fracture appeared to increase with the time-temperature of the heat treatment.

Because of the second etch requirement some additional contraction may have been induced by whatever stress pattern remained in the fiber after etching and heat treatment. Nevertheless, for the limited data given in Table I it appears that the correlation between the axial fiber contraction $\bar{\epsilon}_z$ and the increase in core flaw fracture strain $\overline{\Delta\epsilon_F^c}$ continues to hold at least up to 915° C. The Table I results also suggest that bulk flaws in the boron sheath have ϵ_F greater than 1.4 % and that at least for short times at 1100° C additional contraction can be exerted on the core flaw without changing its inherent flaw strength.

Heat-Etch Technique

In the course of the previous work, as-received fibers were also subjected to high vacuum heat treatment and subsequent change-in-length measurements. This procedure was followed to assure that the observed contraction only occurred in the etched fibers where residual stresses have been altered. Indeed, no measurable length change was observed in the as-received fibers up to 700° C, verifying the creep recovery model at least to this temperature. However, above 700° C significant contraction in the full diameter fibers did occur in a thermally-activated manner. The results for 60 min treatments are shown by curve B of Fig. 6. Clearly, if the large contractive strains could be translated directly into equal increases in core fracture strain, it should be possible to double commercial fiber fracture strain without any loss in fiber diameter. As previously mentioned this desired effect can be obtained only if certain conditions are met, namely, elastic behavior of the core flaw, inherent sheath flaws of high strain-to-failure, and no new flaws introduced by the treatment method. Of course, since the as-received fibers still contained manufacturing-induced surface flaws, the necessity of removing surface layers still remained.

The requirements of the heat-etch technique are therefore simply to heat treat commercial 203 μm fibers above 700° C and then etch until all surface flaws are eliminated. It should be pointed out that at the present

time there is no confirmed theory to explain the strong contractions observed with this technique. For this reason it is difficult from a theoretical point of view to distinguish the basic microstructural processes occurring in the etch-heat technique and those in the heat-etch technique. For example, it may be possible that in the latter technique creep recovery is also occurring but that temperatures above 700° C are required because of thermal history details involved in the fiber's deposition and quench. Or, as suggested by the 615° C data of Fig. 6, a large fraction of the etch-heat contraction may be produced by the same mechanism responsible for the heat-etch contraction. Thus, at the present time these two techniques can be only be distinguished in a practical way such as by assigning certain heat treatment ranges, e.g., the etch-heat below 700° C and the heat-etch above 700° C.

Prior to determining fracture effects of the heat-etch technique, a series of kinetic experiments were conducted in order to measure the rate and magnitude of the contraction available by heat treating at high temperature and high vacuum. The axial strain results for 6, 60, and 600 min heat treatments up to 1200° C are plotted as a function of reciprocal absolute temperature in Fig. 8. Included in this plot are the contraction results both for as-received 203 μm and 102 μm boron fibers. At least three specimens were employed for each measurement.

The data of Fig. 8 indicate that although higher contractions can be achieved in the 203 μm fibers, contractions in both the 102 μm and 203 μm fibers are controlled by the same activation energy. That is, for any contractive strain level above 0.2 %, an order of magnitude change in time requires a change in reciprocal temperature which is independent of fiber diameter. To determine this energy Q, one can employ the cross-cut method (8) which states that the times t_1 and t_2 to reach a certain contraction strain at temperatures T_1 and T_2, respectively, are related as

$$\ln \frac{t_1}{t_2} = \frac{Q}{k}\left(\frac{1}{T_1} - \frac{1}{T_2}\right) \qquad (4)$$

For strains from -0.2 to -1.1 %, the best fit Q value for both 102 μm and 203 μm fibers was determined to be 3.1 ± 0.2 ev. Assuming for this same strain range a linear relationship between ϵ_z and $(T)^{-1}$, one can empirically describe the time-temperature dependence of ϵ_z by the relation

$$\epsilon_z = -B \ln(t/\tau) \tag{5}$$

where

$$\ln \tau = \ln \tau_0 + \frac{Q}{kT} . \tag{6}$$

For 203 μm fibers and time t in sec, B = 0.21 % and $\ln \tau_0$ = -21.4; whereas for 102 μm fibers, B = 0.15 % and $\ln \tau_0$ = -22.1. Thus if temperature were held constant, contractions between 0.2 and 1.1 % would follow a ln t dependence.

Regarding fracture data in full diameter fibers heat-treated in high vacuum, it was necessary first to remove both as-received surface flaws and treatment-induced surface crystals. As previously mentioned the depth of these crystals below the fiber surface increased with increasing time-temperature. Thus the greater the contraction, the deeper the crystal growth. Crystal removal was attempted both with the nitric acid chemical etch and the electrolytic solution employed by Behrendt (3). Both methods were successful but in different ways. For example, the etch removed the crystal at a faster rate than the normal appearing boron surface around the crystal. Thus immediately after crystal removal, the fiber surface was plotted with holes where the crystals had been. If the depth of these holes was not too great, further etching could smooth the surface before the 100 μm diameter was reached. On the other hand, electropolishing appeared to barely effect the crystals so that as boron layers were removed the crystals began to protrude more and more until they were entirely exposed and fell off due to removal of their last contact to the remaining fiber. In this method also, further polishing was required to smooth surface irregularities.

The net effect of requiring a 100 μm limit on etched diameter and removing all flaws associated with crystal growth was that core-initiated fracture could only be observed in fibers with contractions up to about 0.4 %. Indeed, as indicated in Table I under the Heat-Etch Vacuum Heading, fibers with contractions below this level did show the expected rise in fracture strain. For determining the residual stress the effects on ϵ_z after heat treatment, the contraction data of Benrendt (6) such as shown in curves B and C of Fig. 4 were employed. It should be also noted from Table I that even with the detrimental effects of high vacuum, it appears possible to achieve 1.3 % fracture strain by heat treating and removing only about 30 μm off the as-received diameter.

For the heat-etch technique to be effective, it was clear that the surface crystal problem had to be eliminated. A survey of boron fiber experiments in the literature indicated no such problems when the fiber environment was argon gas rather than high vacuum. Gillespie (9), for example, finds that surface migration and thus crystal nucleation can be inhibited by the presence of argon gas at 50 torr. For this reason an experimental setup was developed in which as-received 203 μm fibers could be resistance heated in an argon environment and changes in their length monitored continuously.

The apparatus similar to commercial deposition reactors and that employed by Mehalso (10) is shown schematically in Fig. 9. Stainless steel caps at each end of a 25 mm o.d. pyrex tube provided gas ports for the argon and mercury reservoirs for electrical contact to the boron sheath. End resistances due to current passage from the mercury through the sheath to the tungsten boride core and back again amounted to about 250 Ω. Current was provided by a voltage regulated dc power supply with 2 % ripple. The pyrex tube length and thus the heated-fiber length was varied between 16 and 60 cm to determine and eliminate any end effects from resistance and axial strain measurements. For the latter measurements the fiber was clamped at the top end cap and subjected to a minimal clamp weight of 9 grams below the lower cap. Fiber length changes due to thermal expansion and heat-induced contraction were measured at bottom fiber end with a

traveling microscope. The flow rate of nominally pure argon (99.995 %) was varied between 20 and 200 cc/min at one atmosphere with no apparent effects on thermal expansion or heat-induced contraction.

Fiber temperature above 750° C was measured with an optical pyrometer corrected for an assumed boron emissivity value of 0.55 (9, 11). For temperature determination below the pyrometer range, thermal expansion strain data was taken above 750° C and fitted with a theoretical expansion curve calculated for amorphous boron from Gruneisen's equation (4). This best fit curve shown in Fig. 10 was then employed with low temperature expansion measurements to determine temperature below 750° C. For the range of fiber lengths and gas flows employed here, the temperature of the 203 μm fibers was found to depend only on current in the manner shown in Fig. 11. Thus both thermal expansion strain and fiber current could be used as temperature monitors. Near 1000° C the thermal gradient along the fiber was measured to be less than 20° C; whereas the thermal gradient from core to fiber surface was estimated to be less than 10° C. This estimate was based on the upper limit thermal gradient to be expected if it is assumed that all the measured power input of ~1 watt/cm were developed in a 17 μm core surrounded by a 203 μm boron sheath with thermal conductivity of 25 mw/°C-cm (12). When all errors are considered, the temperature data of Figs. 10 and 11 are estimated to be correct to within ±30° C.

For the measurement of thermally induced contraction in argon, the fiber temperature was quickly (~10 sec) increased from room temperature to heat treatment temperature where its length was monitored as a function of time. Again thermally activated contraction was observed as indicated by the typical results of Fig. 12. At the conclusion of the run, current was quickly (~10 sec) dropped to zero. The change in fiber length measured at high temperature was in exact agreement with the change in fiber length measured at 22° C after thermal treatment, thereby indicating no contraction effects on thermal expansion.

Comparison of Figs. 6 and 12 indicates a significantly faster contraction rate in the argon than in the high vacuum environment. To determine the source of this difference, the times to reach certain contraction strains

were measured as a function of reciprocal temperature. From the resulting data shown in Fig. 13, a Q value of 1.3 ev was determined by Eq. (4) as the best fit energy controlling initial contraction up to 0.2 %. As contraction proceeded above 0.2 %, the Q value decreased, leveling off at 0.84 ev in the 0.3 to 0.8 % strain region. At these higher strain levels, contraction versus time curves at constant temperature did not reproduce well from specimen to specimen. For this region, Q had to be measured by the change of slope method on individual fibers (8). Although the time curves for these fibers differed somewhat, the 0.84 energy determined by the slope method was found to be reproducible.

The faster contraction rate in an argon environment can therefore be explained in most part by a drop in energy from 3.1 ev to about 1 ev. A possible source of the Q drop is suggested by the residual stress pattern data (6) given in Fig. 4. In this plot, curve A is the pattern remaining after 60 min at 1030° C in high vacuum (ϵ_z = -0.4 %) and curve B is the pattern remaining after 180 min at 900° C in argon (ϵ_z = -0.8 %). Although contraction strains differ, the general trend to be observed is that the fiber surface remains in compression after vacuum treatment but actually goes into tension after argon treatment. The argon surface effect is similar to the residual stress effects observed in the etch technique. That is, the presence of argon somehow eliminates compressive surface layers, thus permitting inner tensile layers to relax by contracting. Thus, the higher contraction rate in argon may be caused by the cummulative effect of two mechanisms; i.e., the high vacuum mechanism and the etch-heat mechanism without the etch requirement.

Besides offering faster contractions, the heat-etch technique with argon also offered the desired result of no surface crystals. In fact, for a contraction of 0.8 %, scanning electron microscope photos of heat-treated fibers showed no visible change in surface morphology. However, it did appear that fiber diameters may have decreased by 0.3 ± 0.3 %, suggesting that, in contrast to the anelastic recovery mechanism of the etch-heat contraction, the basic mechanism responsible for the heat-etch contraction may be densification of the amorphous boron sheath. Although the surface appeared unchanged by the argon treatment, flexural strength tests indicated a significant drop in

surface strength. This effect might be explained by tensile surface state indicated in curve B of Fig. 14 and/or the diffusion into the fiber surface of small concentrations of impurity gases such as oxygen. Thus, even with the argon, etching was required to assure core-initiated fracture.

As indicated in the preliminary fracture results of Table I, the weak surface layers of 203 μm fibers heat-treated in argon did not extend below ~150 μm at which diameter core-flaw fractures were observed. For low time-temperature conditions, it is also clear that the observed ϵ_z contractions were indeed experienced by the core flaw. However, for high time-temperature conditions, e.g., 900^{o} C (45 min), low strain core-initiated fractures were observed, suggesting changes in the core flaw. From the scant data available, it appears that perhaps a new type of core flaw (Table I data in parentheses) was introduced which has a strain-to-failure of 0.80 % in the uncontracted fiber. When the fiber contracts, this new core flaw experiences the contraction and thus initiates fracture at a correspondingly higher strain. Therefore, although the heat-etch technique in argon can extend fracture strains to 1.4 % without the crystal problems of high vacuum, it too has its own problems which may be associated with the purity of the argon gas and/or with the method of resistance heating. Near 1000^{o} C, for example, about 50 % of the current was carried by the core. Nevertheless, the heat-etch treatment in an inert gas appears now to offer the best hope of extending ϵ_F above 1.4 % since simple methods for improving purity and eliminating internal heating do exist.

DISCUSSION

The results of Table I confirm the general approach taken here for increasing the strain-to-failure of boron fibers deposited on a tungsten substrate. That is, once surface flaws are removed from 203 μm commercial fibers, flaws within the region of the tungsten boride core become essentially the only source of fiber fracture. Thus any compression exerted on the core flaw by contraction of the boron sheath results in an increase in fiber fracture strain equal to the contraction strain.

The sources of sheath contraction achieved with the techniques discussed here are internal stresses which are a natural consequence of the manufacturing process. In general it appears that these internally-induced contractions are all irreversible in that any core flaw contractions achieved for thermal conditions employed here should not diminish in the temperature use range currently envisioned for boron fibers. Indeed, both the etch-heat and heat-etch techniques require high temperature heat-treatments to attain even stronger contraction. This behavior can be contrasted with possible sheath contraction techniques suggested by DiCarlo (4) that employ external stresses to compressively creep the sheath at high temperature. With these methods, because of the anelastic nature of the boron, any use temperatures near the heat treatment temperature can result in anelastic creep recovery, thereby giving rise to fiber elongation and fracture strains closer to their original values before treatment. There may be, however, many instances where composite production and use temperatures do not approach those temperatures at which fiber contraction by external means was achieved.

Regarding commercial practicality of the techniques discussed here, it is clear that until the sources of surface flaws are eliminated, the etch process or its equivalent must be an essential element of any method that desires to make a significant improvement in boron fiber fracture strain. As Smith (2) has found, the depth of surface removal for the as-received fibers is minimal, probably of the order of 5 μm (0.2 mils). Considering the etch-induced change in average fracture strain from 0.9 % to 1.1 %, in coefficient of variability from >20 % to <5 %, and in minimum fracture strain from 0.5 % to 1.0 %, it would seem that this additional fiber processing is more than cost effective, especially for those composite areas requiring high impact resistance without fiber breakage.

Pursuing the etch process beyond the initial surface layers as in the etch technique is another story, however. Down to the 100 μm level residual stress pattern effects do achieve about an additional 0.2 % increase in strain-to failure, but at the significant expense of removing some 75 % of the boron sheath. Considering the fact that the heat-etch technique can in this early stage of development accomplish equivalent strain improvement with much

less loss of boron sheath, it is clear that both the etch and etch-heat techniques are not practically feasible at the present time. This conclusion may be altered somewhat in the future, if, for example, deposition methods are developed which significantly increase the gradient in the residual surface stress pattern (cf. curve A, Fig. 3). The increased gradient should permit much stronger contractions for much less removal of the boron sheath.

For cost effectiveness it thus appears that of the three techniques studied in this report, the heat-etch method of heat treating commercial boron-on-tungsten fibers offers the best approach toward significantly increasing fiber fracture strain. This conclusion is based primarily on the hope that this technique can be developed to the point where little loss of boron sheath is required in order to achieve core-initiated fracture. Because the high vacuum technique is beset with surface crystal problems as well as the practical problems associated with continuous fiber processing, primary attention should be directed toward inert gases for the heat treatment environment. Commercial setup for fiber preparation would seem then only to require a second in-line reactor such as that shown in Fig. 9. At the present time the use of resistance heating to provide the power input for the heat treatment is questionable. If this particular heating method proves undesirable, the second reactor might be replaced by a tube furnace. In fact, such secondary fiber treatment has been reported by Camahort et al (13) in which 143 μm fibers were passed through oxygen and ammonia gases near 1000^{o} C to form a boron nitride coating. Indeed, these investigators report a fracture stress increase of 130 ksi, at least part of which might be explained by the high temperature contractions observed here.

Data regarding optimum parameters and capabilities of the argon heat etch technique are scant at the present time. From the high vacuum work, contraction strains as high as 1.1 % seem to be available. The Table I results suggest, however, that high contraction strains must be achieved in a minimum of time in order to avoid the appearance of new thermally-induced flaws. Although contraction kinetics with very pure argon gas have not been determined above 1100^{o} C as yet, one might assume contractions similar to the high vacuum results of Fig. 8. For upper practical limits of 6 min and

1250° C for the heat treatment conditions, Fig. 8 indicates a contraction strain of ~0.8 % should be achieved. Thus, it may not be unreasonable to employ the heat-etch technique to produce fibers with fracture strains near 1.9 % and room temperature fracture stresses above 7 GN/m^2 (1000 ksi).

As in most basic studies, this preliminary investigation of high temperature contraction raises more questions than it answers. For example, how are contraction kinetics and residual stress patterns affected by other gases, such as those employed in deposition? Indeed, how much contraction does occur during the actual deposition process? What is the physical relationship between the contraction mechanism and the elongation mechanism observed during deposition? What is the source of the difference in the energies controling contraction in vacuum and in argon? What is the role of resistance heating in the contraction kinetics and possibly in the introduction of new flaws? What are the time-temperature limits below which the original core flaw retains its structural integrity and elastic behavior? Finally, what are the effects of internally-induced axial contraction on fiber transverse strength? Future work will attempt to answer these questions with the hope that the full mechanical capabilities of boron fibers can be achieved.

SUMMARY OF RESULTS

The general approach taken here was based on the premise that flaws associated with the tungsten boride core in CVD boron fibers could be contracted to produce a corresponding increase in fiber fracture strain. This approach applied to commercial 203 μm (8 mil) fibers was verified by the fracture results of three contraction techniques which employ etching and thermal processing. In all cases, internal stresses available in the CVD boron sheath were used to achieve core flaw contraction. The etching process was a necessary element of each method in order to eliminate both commercial and treatment-induced surface flaws and thus assure core-initiated fracture. The heat-etch technique in which as-produced fibers were reheated above 700° C appears to be the most cost-effective on account of minimal boron sheath

removal required during subsequent etching. Preliminary results indicate that with this technique fracture strains of 1.4 % can be achieved near final diameters of 170 μm. At the present time, it is uncertain what heat treatment environment is optimum for achieving maximum contraction in minimal time with minimal new flaw production. Results for both vacuum and argon environments show a large disparity in both contraction kinetics and unetched fracture behavior. Future work must necessarily concentrate on this particular environmental problem because preliminary data suggest that the heat-etch technique may be capable of achieving enough core contraction to produce large diameter fibers with fracture strains over two percent and fracture stresses well over 7 GN/m^2 (1000 ksi).

REFERENCES

1. F. E. Wawner and D. B. Satterfield: Appl. Phys. Lett., 1967, Vol. 11, pp. 192-194.
2. R. J. Smith: NASA Tech Note D-8219, Washington, D.C., 1976.
3. D. R. Behrendt: Fourth Conference on Composite Materials: Testing and Design, Am. Soc. for Test. Mater., Philadelphia, 1977, pp. 215-226.
4. J. A. DiCarlo: Fourth Conference on Composite Materials: Testing and Design, Am. Soc. for Test. Mater., Philadelphia, 1977, pp. 443-465.
5. J. A. DiCarlo: Scr. Metall., 1976, Vol. 10, pp. 115-119.
6. D. R. Behrendt: Private communication.
7. R. M. Witucki: Air Force Materials Lab., AFML-TR-66-187, Wright-Patterson Air Force Base, Ohio, 1967.
8. A. C. Damask and G. J. Dienes: Point Defects in Metals, Gordon and Breach, New York, 1963.
9. J. S. Gillespie, Jr.: J. Am. Chem. Soc., 1966, Vol. 88, pp. 2423-2425.

10. R. M. Mehalso: Ph.D. Thesis, Rensselaer Polytechnic Institute, Troy, New York, 1973.

11. R. J. Diefendorf: Private communication: boron emissivity = 0.50 ±0.05.

12. O. A. Golikova, et al.: Phys. Status Solidi. (A), 1974, Vol. 21, pp. 405-412.

13. J. L. Camahort, V. J. Krukonis, and F. E. Wawner: SAMPE Q, 1975, Vol. 6, pp. 40-43.

TABLE I. - FRACTURE RESULTS FOR TREATED 203 μm BORON FIBERS

Technique	D_1[a], μm	Thermal treatment	D_2[b], μm	$\bar{\sigma}_F(q_0)$, GN/m²	ksi	$\bar{\epsilon}_F$, %	$\bar{\epsilon}_z$, %	$\Delta\bar{\epsilon}_F$[c], %
As-received	203			3.59	521	0.92		
Etch	198	None	198	4.38	635	1.12	-0.01	≡0.01
	102	None	102	5.08	737	1.30	-0.17	0.19
Etch-Heat	104	500° C (60 min)	104	5.39	782	1.38	-0.20	0.27
	127	800° C (0.5 min)	109	5.43	788	1.39		
	152	800° C (90 min)	112	5.21	755	1.33		
	104	915° C (60 min)	89	5.33	773	1.36	-0.34	0.25
	127	1100° C (0.5 min)	107	5.59	810	1.43		
Heat-Etch Vacuum	203	915° C (60 min)	180	4.90	710	1.25	-0.15	0.14
			97	5.09	738	1.30	-0.20	0.19
	203	1030° C (60 min)	100	----	---		-0.50	
	203	1100° C (6 min)	180	----	---		-0.29	
			117	5.57	808	1.42	-0.34	0.31
Heat-Etch Argon	203	785° C (60 min)	203	----	---		-0.18	
			152	5.13	744	1.31		0.20
			152	(3.90)	(566)	(1.00)		(0.20)
	203	900° C (45 min)	203	----	---		-0.38	
			152	(4.67)	(677)	(1.19)		(0.39)
	203	1050° C (10 min)	203	----	---		-0.34	
			170	5.50	798	1.40		0.29

[a]Fiber diameter after initial etch and before thermal treatment.

[b]Fiber diameter after thermal treatment and final etch.

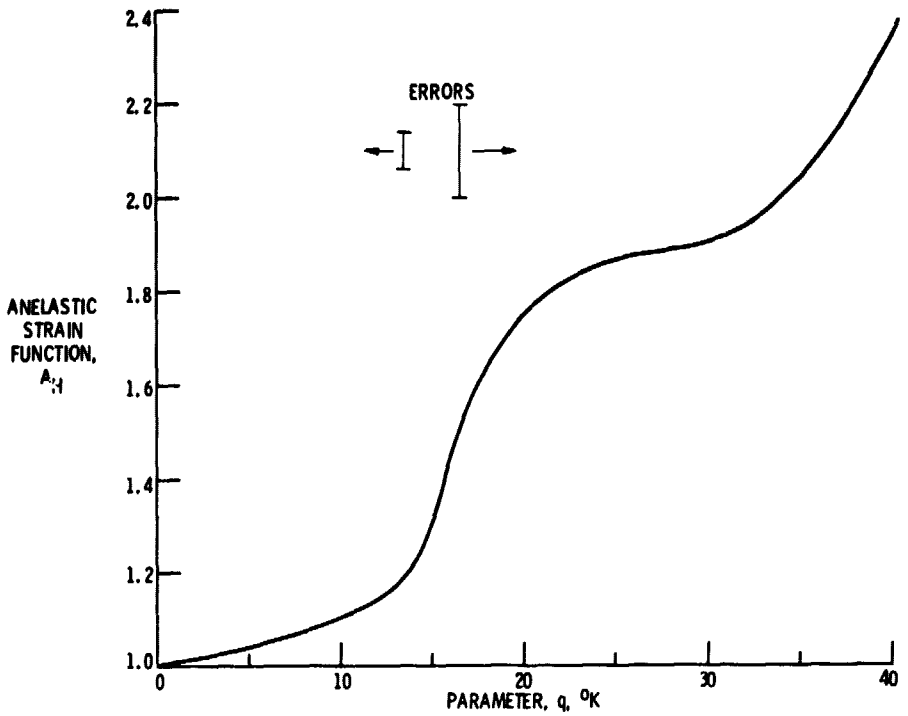

Figure 1. - The dependence on the time-temperature parameter q for the high stress anelastic strain function A_H of boron fibers (4).

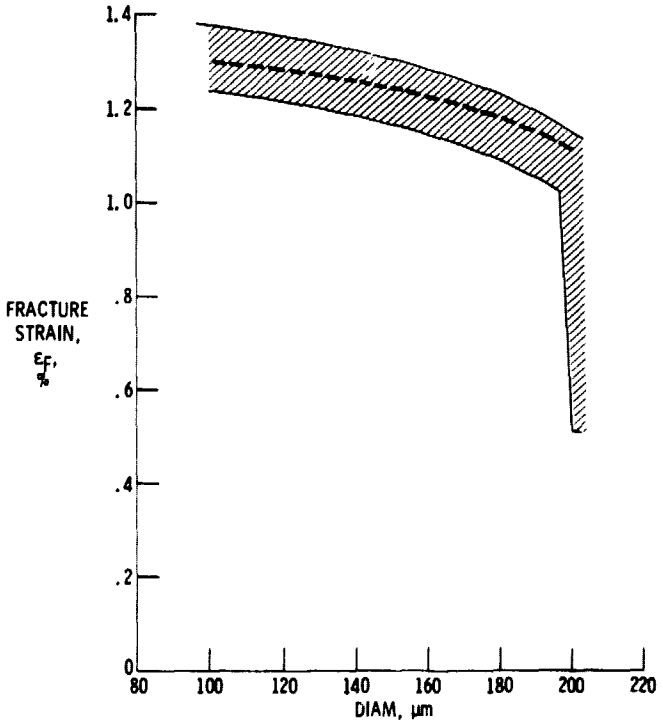

Figure 2. - Range of fracture strain for 203 μm (8 mil) as-received boron fibers as a function of diameter reduced by etching (2). The dashed line is the average fracture strain determined by adding the etch-induced contraction strain (curve A, fig. 4) to 1.11 percent, the average core-initiated fracture strain at full diameter.

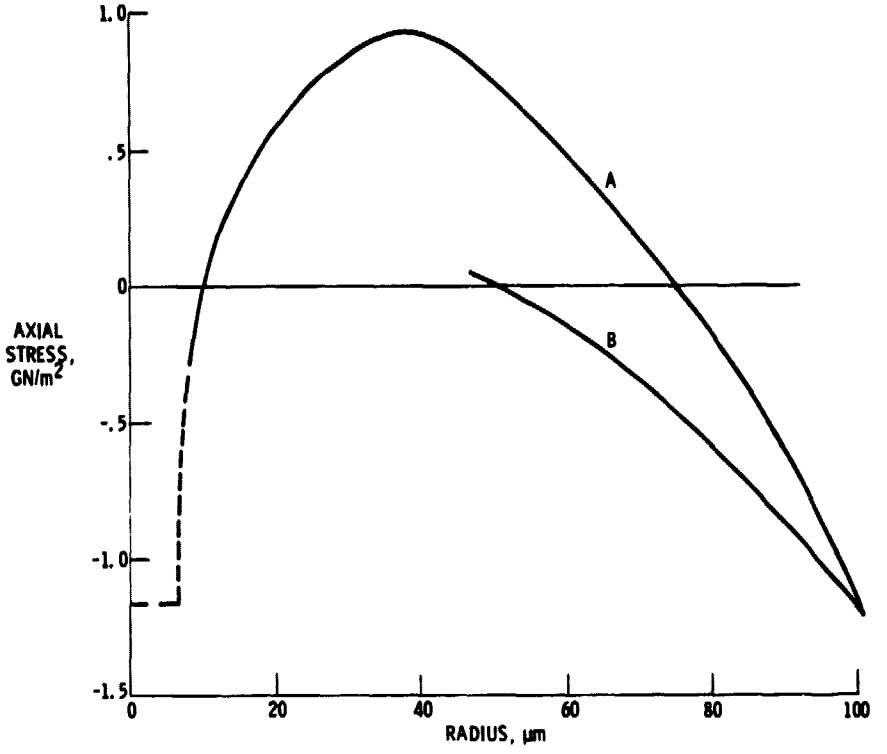

Figure 3. - Curve A: Typical axial residual stress distribution in 203 μm as-received boron fibers. Curve B: Axial surface stress in these fibers as a function of radius reduced by outer layer removal (6).

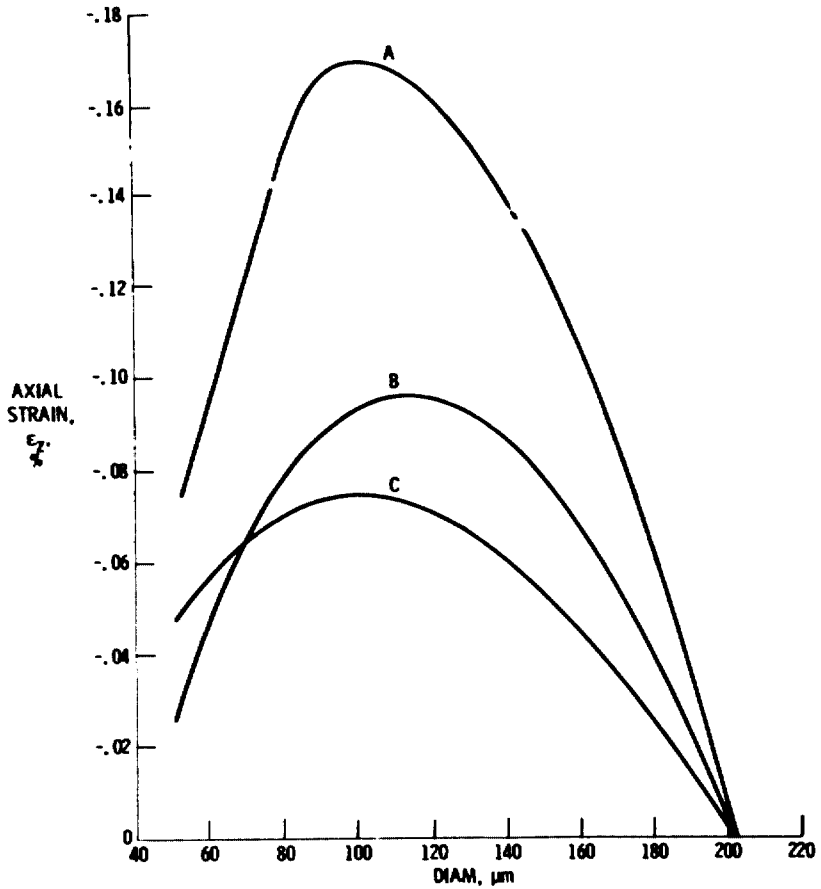

Figure 4. - Typical axial strain as fiber diameter is reduced by outer layer removal. Curve A: 203 μm as-received boron fibers. Curve B and C: 203 μm fibers after high vacuum heat treatment for 60 min at 915° C (curve B) and 1030° C (curve C).

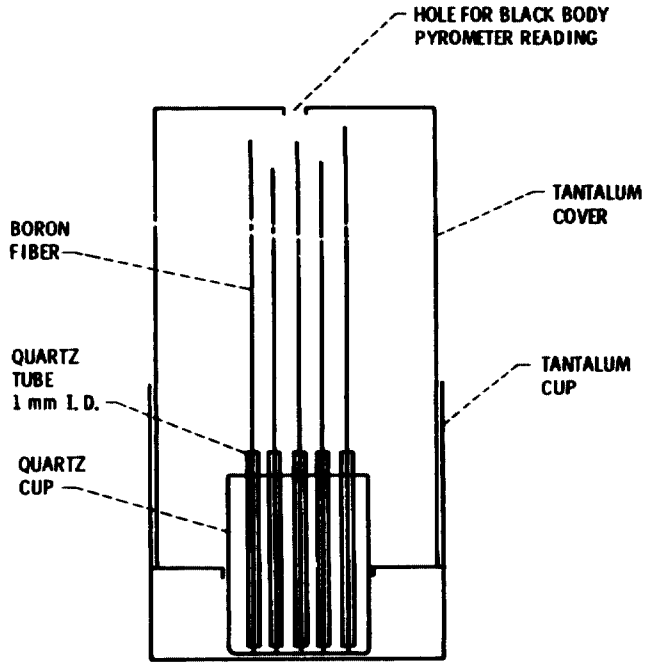

Figure 5. - Schematic of apparatus for heat treating boron fibers in high vacuum furnace.

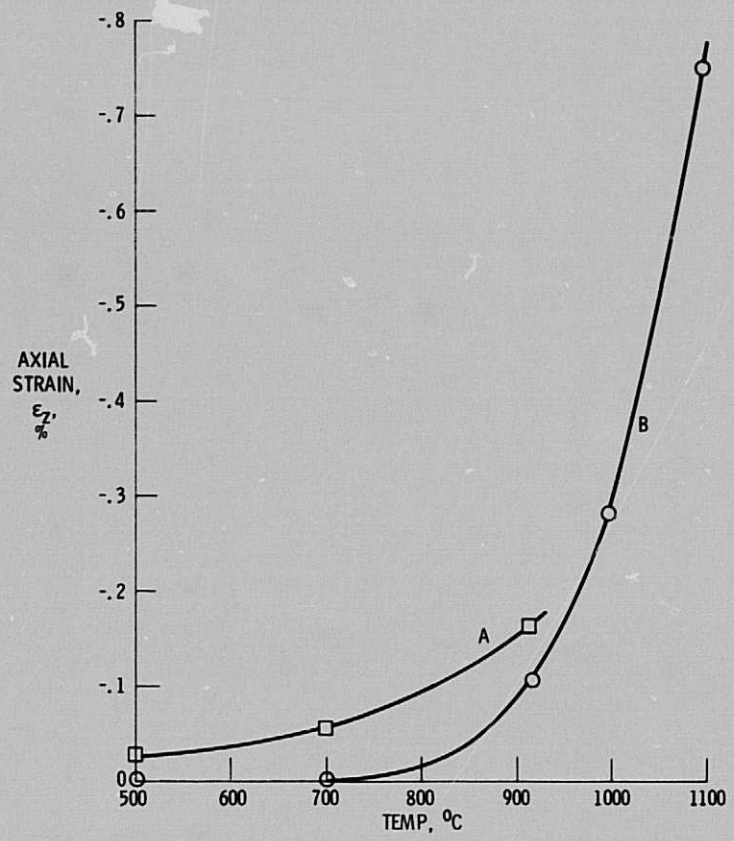

Figure 6. - Axial strain as a function of temperature for 60 min heat treatments in high vacuum. Curve A: 203 μm as-received boron fibers etched to 104 μm before heat treatment. Curve B: 203 μm as-received fibers.

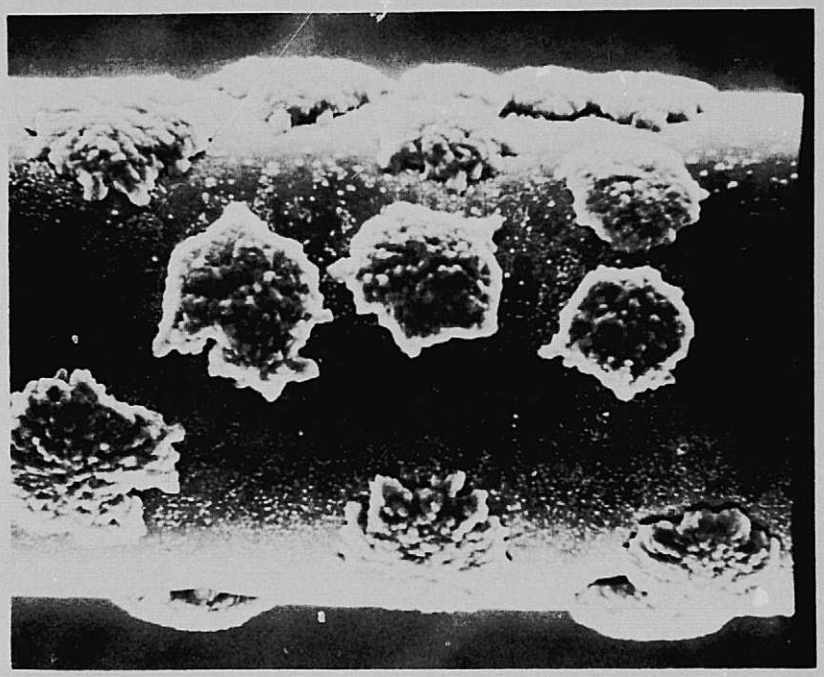

Figure 7. - Scanning electron microscope photograph of typical surface crystal growth induced by heat treating both etched and unetched boron fibers in high vacuum ($<10^{-7}$ mm Hg). Actual photo is 203 μm as-received fiber after 60 min at 1200^{0} C.

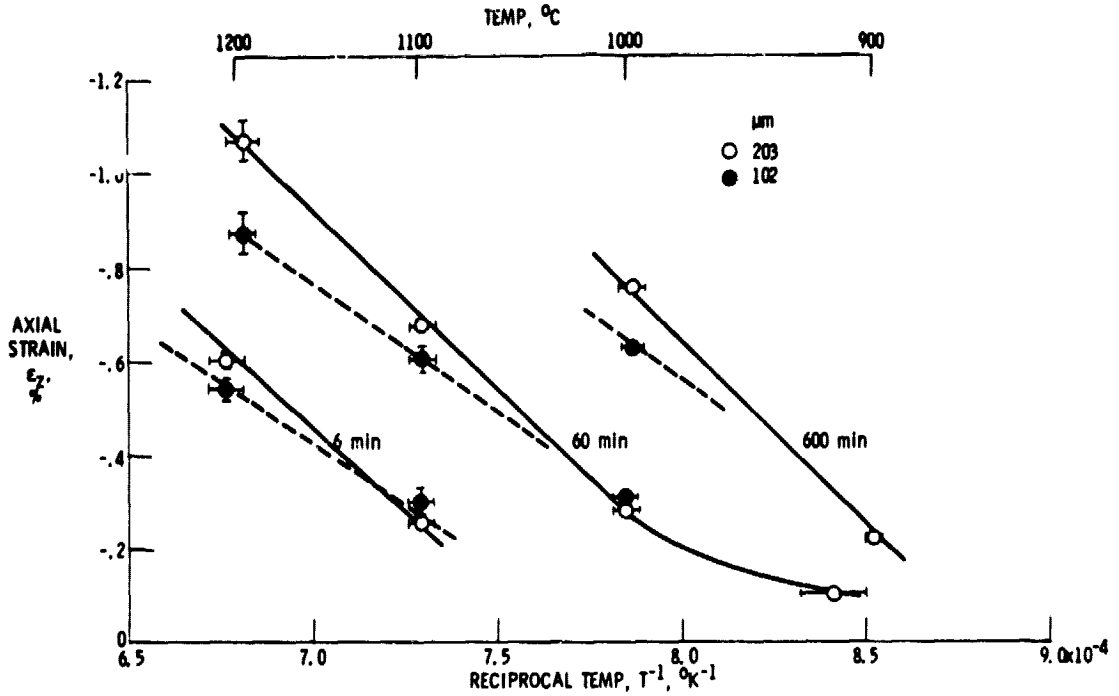

Figure 8. - Axial strain for 203 μm and 102 μm as-received boron fibers after high vacuum heat treatment for the indicated times and temperatures.

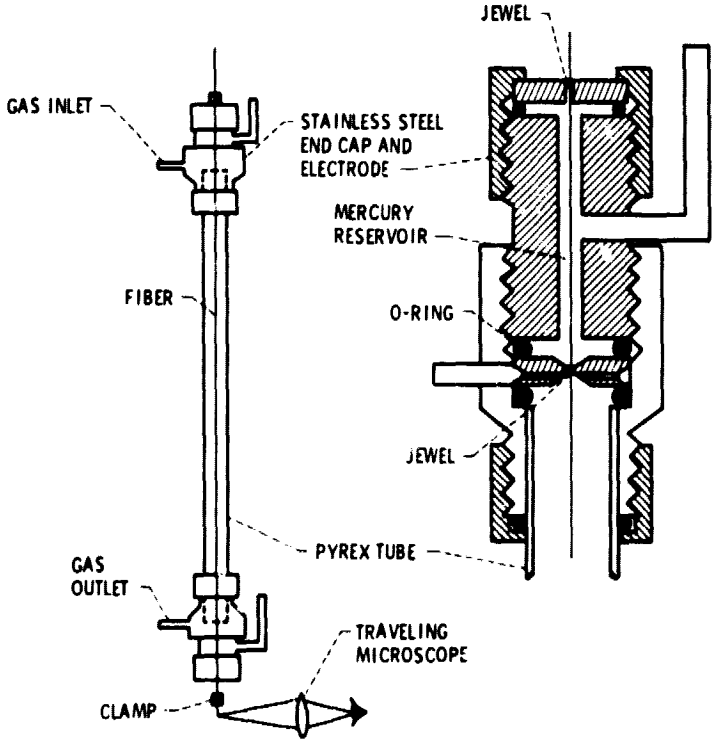

Figure 9. - Schematic of apparatus employed to heat treat 203 μm boron fibers in a gas environment and simultaneously measure changes in fiber length.

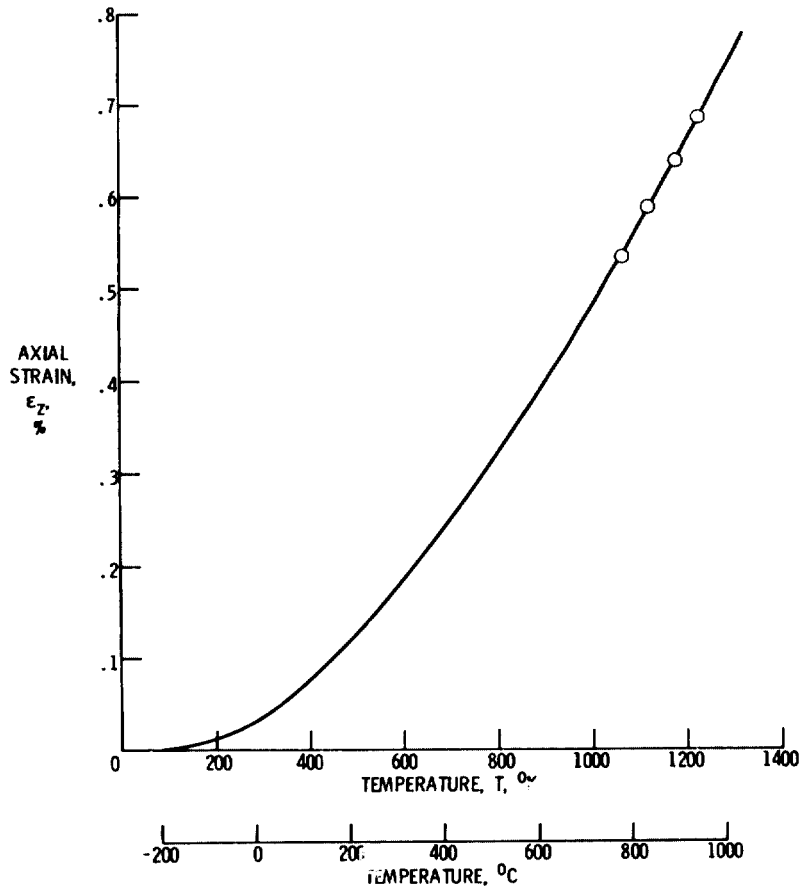

Figure 10. - Thermal expansion strain of 203 μm as-received boron fibers as empirically determined by fitting the high temperature data points to Gruneisen's equation for the thermal expansion coefficient of amorphous boron.

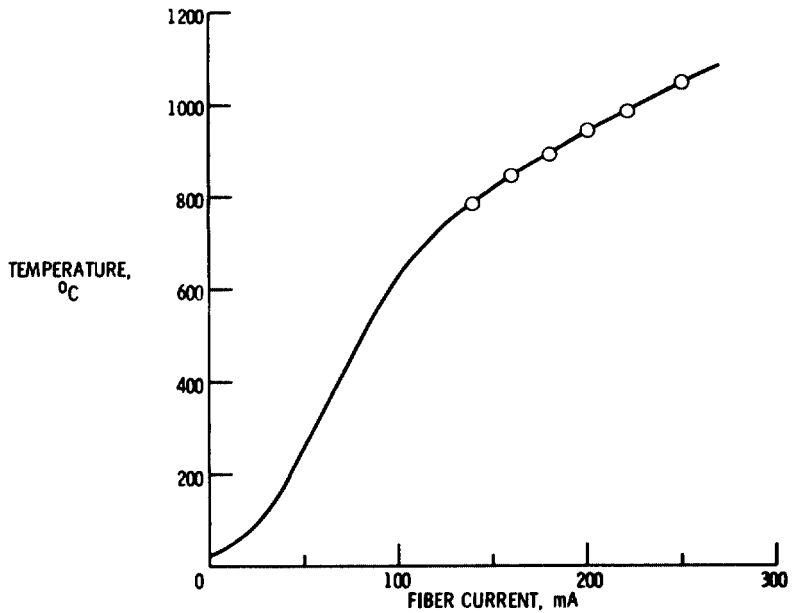

Figure 11. - Temperature of 203 μm boron fibers as a function of fiber current for 1 atmosphere of argon gas in the reactor of figure 9.

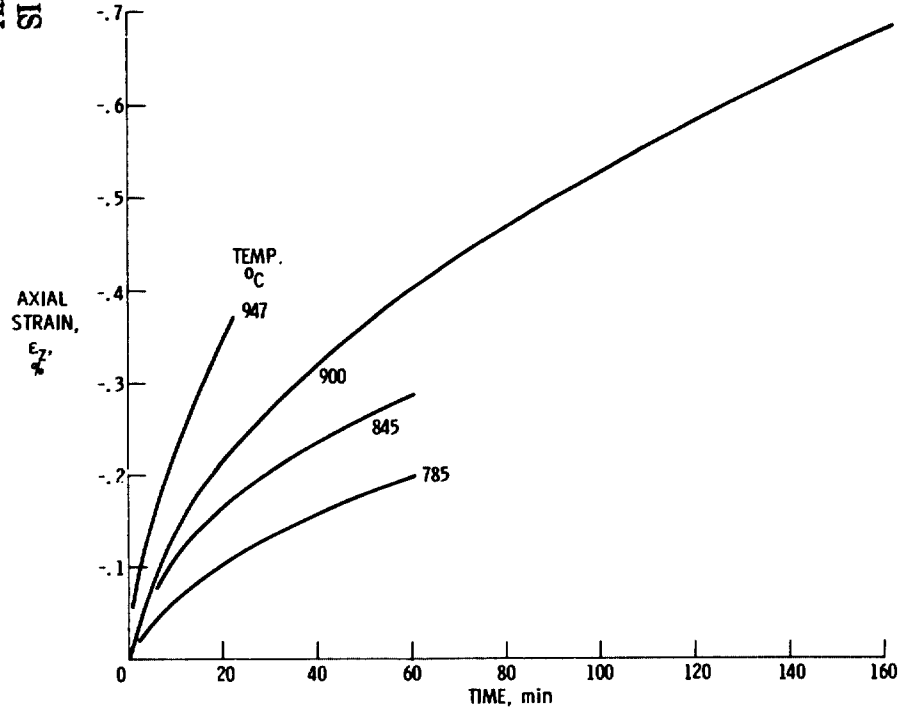

Figure 12. - Typical time-temperature dependence of the axial strains observed in 203 μm as-received boron fibers during heat treatment in argon gas.

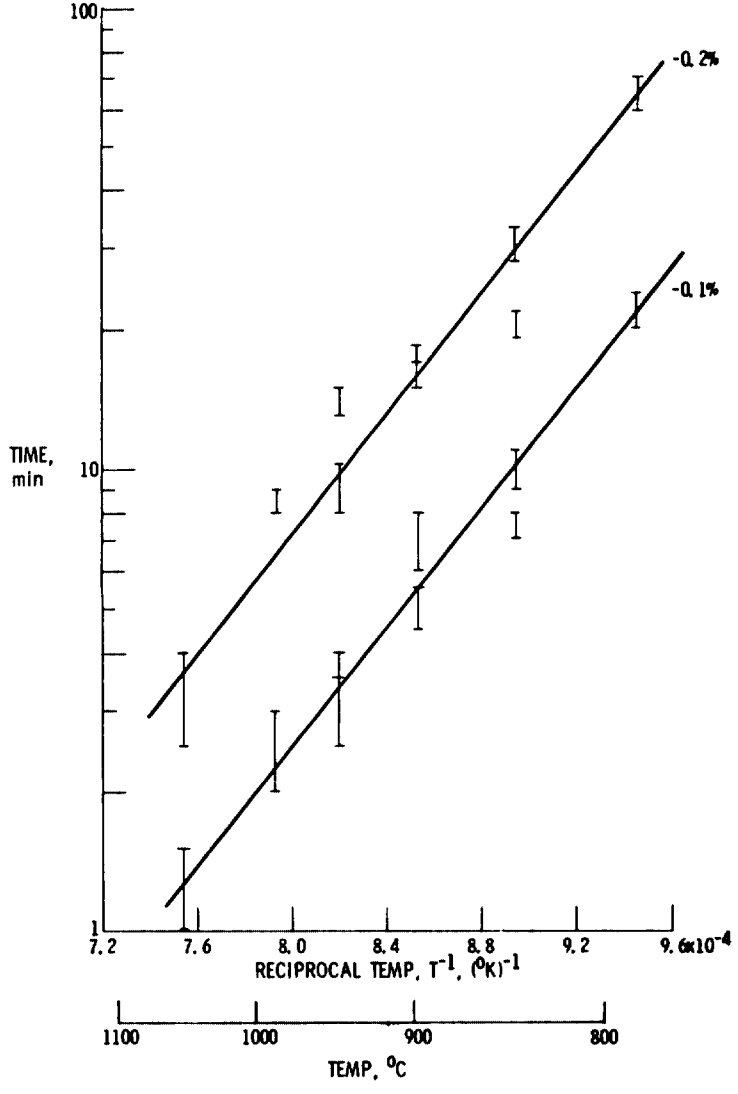

Figure 13. - Times and temperatures to achieve 0.1 and 0.2 percent axial contraction strains in 203 μm as-received boron fibers heat treated in argon gas.

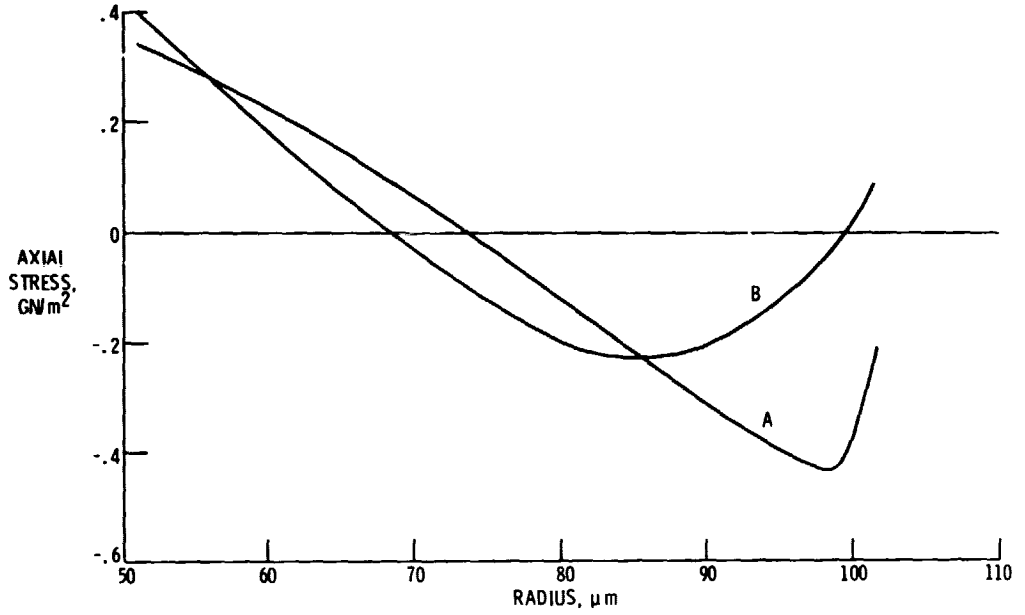

Figure 14. - Typical axial residual stress distributions in 203 μm as-received boron fibers after heat treatment. Curve A: 60 min at 1030° C in high vacuum. Curve B: 180 min at 900° C in argon.

E-5119